Complex synchronization structure of an overdamped ratchet with discontinuous periodic forcing

D. G. Zarlenga,[1] H. A. Larrondo,[1] C. M. Arizmendi,[1] and Fereydoon Family[2]
[1]*Departamento de Física, Facultad de Ingeniería, Universidad Nacional de Mar del Plata, Avenida J.B. Justo 4302, 7600 Mar del Plata, Argentina*
[2]*Department of Physics, Emory University, Atlanta, Georgia 30322, USA*
(Received 11 February 2009; published 22 July 2009)

A deterministic overdamped ratchet driven by a periodic square driving force is shown to display chaotic behavior. The system has neither temporal nor quenched noise but the strong nonlinearity of the driving force produces a very rich bifurcation pattern with synchronized as well as chaotic regions. This pattern disappears if a sinusoidal force replaces the square force. This unexpected behavior is explained by decomposing the system into two exactly solvable subsystems, each with its own characteristic transit time, so that the ratio between the period of the driving force and the transit times can be analyzed. The transition from synchronized to chaotic motion can be explained by means of a one-dimensional Poincaré map. Our results can be experimentally confirmed in a number of systems, including the three-junction superconducting quantum interference devices ratchet, the rocking ratchet effect for cold atoms, and the Josephson vortex ratchet.

DOI: 10.1103/PhysRevE.80.011127 PACS number(s): 05.60.Cd, 05.45.Ac

I. INTRODUCTION

The ratchet effect was initially proposed as a model for molecular motors [1,2], but more recently considerable theoretical and experimental works on ratchets have appeared in a wide range of other areas not only in physics and engineering but also in social sciences [3]. For example, Gommers *et al.* [4] used an overdamped ratchet model to investigate the route to quasiperiodicity in an experimental study of cold atoms; the driven motion of domain walls in extended amorphous magnetic films was experimentally studied and theoretically described using an overdamped two-dimensional (2D) ratchet effect [5,6]; voltage rectification by a superconducting quantum interference device (SQUID) ratchet was predicted by Zapata *et al.* [7]; and the three-junction SQUID was experimentally and theoretically studied by Sterck *et al.* [8]. A ratchet effect was experimentally found by Carapella and Costabile [9] in a relativistic flux quantum trapped in an annular Josephson junction embedded in an inhomogeneous magnetic field, and it was explained using an overdamped ratchet with a rectangular periodic force. The transport of magnetic flux quanta (vortices) in superconducting devices was investigated in [10,11] and recently a deterministic underdamped Josephson vortex ratchet was also experimentally studied by Beck *et al.* [12].

The nature of the driving force plays a key role in the ratcheting behavior. Recently, a number of different types of periodic forcing have been considered in the study of ratchets. Kostur *et al.* [13] found a rich variety of anomalous transport by applying both a time-periodic (ac) and a constant biasing (dc) current to a Josephson junction device. Biharmonic driving has been studied in optical lattices [14] and a periodic alternating delta function was considered in [15]. Lade [16] studied a wide class of driving functions in order to answer the question of optimal driving force in overdamped ratchets, which is defined as the driving function that achieves a maximum velocity. Lade [16] found that optimal driving wave forms are dichotomous. Chaudhuri *et al.* [17] also studied an overdamped ratchet using a Langevin equation with multiplicative noise. Using this approach, they explored the possibility of observing a phase-induced current as a consequence of state-dependent diffusion. Machura *et al.* [18] studied transport in an overdamped Brownian motor moving in a ratchet potential that is driven by thermal and dichotomic nonequilibrium noise in the presence of an external constant load force in both the classical and the quantum tunneling regimes. Finally, Air and Liu [19] studied the effect of reduced dimensionality in an overdamped Brownian particle moving along the axis of a three-dimensional periodic tube. They found that the reduction in the spatial dimensionality leads to the appearance of not only an entropic barrier but also an effective diffusion coefficient.

Two phenomena that have received less attention in the study of ratchets are the synchronization and the chaos. The synchronization of overdamped ratchets was studied by Alatriste and Mateos [20] and the underdamped case was considered in [21].

Synchronization appears in many problems concerning oscillators and resonators [22]. Inertial and overdamped ratchets are, respectively, included in these two classes because inertial ratchets and oscillators share the same equation, with the only difference that time is considered as a $\mathbb{R}^1$ variable for ratchets instead of the $\mathbb{S}^1$ variable used in oscillators; in a similar way, overdamped ratchets are equivalent to resonators. Both inertial and overdamped ratchets have an asymmetric potential energy producing ratchet force with zero spatial mean value. Transport is produced by combination of this ratchet force with the periodic driving force, which has zero temporal mean value.

Bifurcations, chaos, and multiple synchronization are typical behaviors of many nonlinear systems. But chaos seems precluded in resonators and overdamped ratchets, even if they are driven by a periodic force, because they are modeled by one or two first-order differential equations. The well-known *existence and uniqueness theorem* of differential equations states that solution exists and is unique for dynamical systems with a C^1-vector field.

As a consequence chaos is precluded for dynamical systems of order <3. The Poincaré-Bendixon theorem also pre-

cludes chaos in 2D systems but it requires a continuous and differentiable 2D-vector field [23].

A possible way to obtain chaos in overdamped ratchets is to make them stochastic. In [24] quenched noise was added to a periodically driven overdamped ratchet and both chaos and anomalous diffusion [25] were obtained with the quenched noise strength as a control parameter. In [26] it was reported that for quenched disorder with long-range spatial correlations, diffusion becomes anomalous, and both the correlation degree and the amount of quenched disorder can enhance the anomalous diffusive transport. The analysis of synchronization of the motion of particles with an external sinusoidal driving force was studied in [27] for both a perfect lattice and a lattice with quenched noise. In the quenched noise case a new trapping mechanism was observed as responsible for the anomalous diffusion. An approximation to the trapping probability density function in a disordered region of finite length included in an otherwise perfect ratchet lattice was obtained in [28].

Another strategy is to increase the dimension by adding an inertia term. This case was studied in several papers (see, for example, [29–38]).

In this paper we propose another way to get a 2D system that may have chaotic behavior: to use a discontinuous periodic force as driving. Then the vector field is no longer C^1 and chaos is not precluded. Trajectories for non-C^1 fields may be discontinuous and chaos and multiple synchronization becomes possible as it is the case for the model studied in this paper. Our model also includes the same ratchet force used in [27]. A periodic square-wave driving force was recently considered by Salgado-García *et al.* [39] in order to obtain the necessary and sufficient conditions that the ratchet potential must satisfy in order to have a vanishing current. Salgado-García *et al.* [40] extended the formalism in order to study the robustness of current reversals in overdamped deterministic ratchets under symmetric forcing. They showed that for the case of a periodic dichotomous forcing, current reversal is not uncommon and exists for a nonzero measure set of the parameter space. They also showed numerically that, for a wide class of ratchet potentials, current reversals also occur when the discontinuous dichotomous forcing is replaced by symmetric continuous driving forces. The importance of rectangular periodic forcing has also been recently considered in [41–44].

The main contribution of this work is to show that in this simple model a rich bifurcation diagram emerges and both synchronized and chaotic regions appear in the bifurcation diagram. Our results complement those obtained by Cubero *et al.* [45], who studied the drift velocity as a function of the driving parameter and who theoretically predicted and numerically confirmed the existence of zero velocity bands. The synchronization pattern we are studying here is confined to only a small region near the origin in their parameter space.

The outline of the paper is as follows. In Sec. II the single-particle model is presented. The bifurcation diagram for the winding number as a function of the amplitude and period of the forcing, as control parameters, is compared with previous results for a sinusoidal driving force [28] in Sec. III. In Sec. IV we analyze the synchronization between the particle motion and the periodic commutation with period $T/2$ using two exactly solvable subsystems. Each subsystem is studied by recourse to standard qualitative theory and characteristic times τ_+ and τ_- (for forward and backward motions, respectively) are analytically obtained. The bifurcation diagram is then explained in terms of the relation between these characteristic times τ_+ and τ_- and the commuting period $T/2$. Furthermore, the boundaries of the synchronization zones are obtained in Sec. V by an analytical argument. A two-step one-dimensional map shows how bifurcations arise. The maximal Lyapunov exponent Λ allows one to verify that the system is chaotic for specific regions in the parameter space. Finally, conclusions are presented in Sec. VI.

II. MODEL

We consider the motion of a particle in a perfectly periodic lattice (without quenched noise) modeled by a forced overdamped ratchet with a square wave as the external periodic force. The dynamical equation is given by

$$\gamma\dot{x} = R(x) + F(t), \tag{1}$$

where γ is the damping coefficient, $R(x) = -dU/dx$ is the ratchet force, and $F(t)$ is the time dependent external force.

As in a number of previous studies, the periodic, asymmetric, ratchet potential [24,28,30,31,45] is modeled by the equation

$$U(x) = -A\left[\sin(2\pi x/\lambda) + \frac{\mu}{2}\sin(4\pi x/\lambda)\right] \tag{2}$$

with the amplitude A and spatial period λ. Two consecutive maxima define a *valley* of length λ. The time dependent external periodic force is modeled by the square wave of the form

$$F(t) = \begin{cases} +\Gamma & \text{if } 0 < t \le T/2 \\ -\Gamma & \text{if } T/2 < t \le T, \end{cases} \tag{3}$$

where Γ and T are the amplitude and the period of the force, respectively.

We used a variable step Runge-Kutta-Fehlberg method [46] technique in order to numerically solve Eqs. (1) and (3). Since we are interested in investigating the influence of parameters Γ and T on the transport properties of the ratchet, we used the same values of the parameters as in previous studies [24,27,28,32,35], namely,

$$A = 1, \quad \lambda = 2\pi, \quad \gamma = 1, \quad \mu = 0.5. \tag{4}$$

It is useful to introduce the following scaled variables for the model (those with tilde are dimensionless variables):

(i) $\tilde{x} = x/\lambda$ is the position of the particle along the ratchet potential.

(ii) $\tilde{v} = v/v_\omega$, with $v_\omega = \lambda/T$, is the velocity. The mean velocity $\langle\tilde{v}\rangle$ gives the ratchet current.

(iii) $x_r = (x \bmod \lambda)$, the reduced position, is the position of the particle inside the potential.

(vi) $x_{1/2}$ is the position reached by the particle at $t = T/2$, starting at x_0, with the external force $F = +\Gamma$.

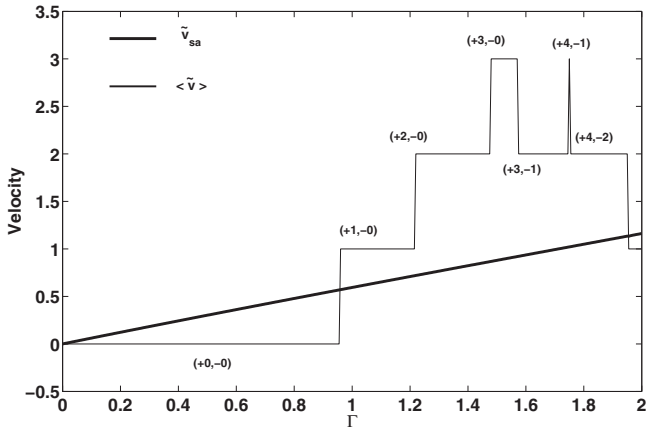

FIG. 1. Sampled velocity $\tilde{v}_{sa}$ and mean velocity $\langle\tilde{v}\rangle$ of a particle in a perfect lattice as a function of Γ for a sinusoidal driving force. The particle starts at $\tilde{x}=0$. Note the jumps in $\langle\tilde{v}\rangle$ at $\Gamma \simeq 0.96, 1.22, 1.47, 1.57, 1.75, 1.76, 1.95$, but $\tilde{v}_{sa}$ has no bifurcations in this range of Γ. The label over each zone indicates the number of valleys crossed by the particle, forward (+) and backward (–), in a period T.

(v) $\{x^{sa}\}$, $\{x_r^{sa}\}$, and $\{v^{sa}\}$, are the sampled position, the sampled reduced position, and the sampled velocity, respectively. They are defined by

$$\{x^{sa}\} = \{x(kT^-), (k = 0, 1, \ldots)\},$$

$$\{x_r^{sa}\} = \{x_r(kT^-), (k = 0, 1, \ldots)\},$$

$$\{v^{sa}\} = \{v(kT^-), (k = 0, 1, \ldots)\}. \quad (5)$$

The superscript "–" in the above definitions indicates that sampling proceeds just before the jump from $-\Gamma$ to $+\Gamma$. Synchronization with the external force is evidenced by the periodic $\{x_r^{sa}\}$ and $\{v^{sa}\}$ time series and consequently these variables may be used to detect synchronization with the external driving force [28].

III. BIFURCATION DIAGRAM

Let us review the results for a sinusoidal driving force $\Gamma \sin(\Omega t)$. Figure 1 corresponds to a perfect lattice (i.e., without quenched noise) [27]. The bifurcation diagrams of $\tilde{v}^{sa}$ and $\langle\tilde{v}\rangle$ as a function of Γ are shown in Fig. 1 for Γ in the range [0,2] and show that $\tilde{v}^{sa}$ is a monotonic and also increasing function of Γ while $\langle\tilde{v}\rangle$ is a step function with jumps at specific values of Γ. As Γ increases the number of valleys traversed by the particle during the positive and negative cycle changes, producing the steps in $\langle\tilde{v}\rangle$. Labels over each step indicate the number of valleys traversed during positive and negative cycles. The motion of the particle remains synchronized with the external force through the entire range [0,2] as it is shown by the single value of $\tilde{v}_{sa}$.

Let us consider now the case of a square wave with amplitude Γ and period T. Figures 2(a) and 2(b) show the bifurcation diagrams for $\langle\tilde{v}\rangle$ and $\tilde{v}^{sa}$ as functions of the control parameter $\Gamma \in [0, 2.5]$ for $T \simeq 15.06\pi$. Diagrams in Figs. 1 and 2 have been obtained by using method I described in

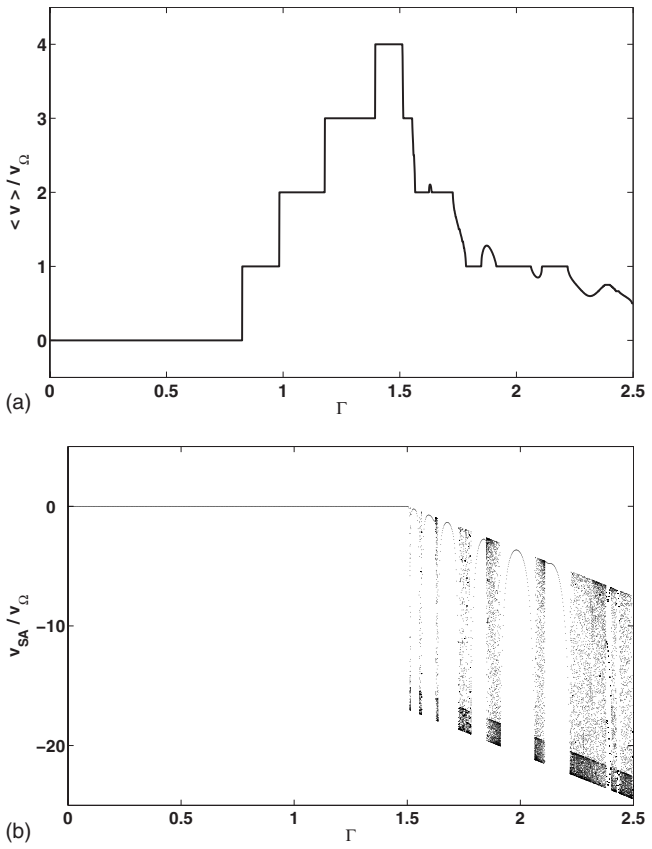

FIG. 2. (a) Mean velocity $\langle\tilde{v}\rangle$ and (b) sampled velocity $\tilde{v}_{sa}$ of a particle as a function of Γ; $T \simeq 15.06\pi$. The particle starts at $\tilde{x}=0$. Note that $\langle\tilde{v}\rangle = 0$ for $\Gamma \leq \mu + 1/(8\mu)$ and v_{sa} has no bifurcations for $\Gamma \leq 1+\mu$.

[33]. In this method the simulation is done by resetting the initial condition to the same value when Γ or T is changed. At higher values of Γ (not shown in Fig. 2) the particle motion becomes oscillatory with a null current because the ratchet force $R(x)$ becomes negligible as compared to Γ. The intervals with constant $\langle\tilde{v}\rangle$ in Fig. 2(a) correspond to the motion of a particle synchronized with the external force. This is confirmed by only one $\tilde{v}^{sa}$ in the bifurcation diagrams in Fig. 2(b).

As will be justified in Sec. IV below, the sampled velocity $\tilde{v}_{sa}$ is zero for $\Gamma < (1+\mu)$, provided the period is long enough so that the particle can reach a stationary state during the negative half cycle of the external square wave. When $\Gamma > (1+\mu)$, the system has both synchronized and nonsynchronized regions in the $[\Gamma, T]$ parameter space. Nonsynchronized regions correspond to intervals in which $\langle\tilde{v}\rangle$ is not horizontal in Fig. 2(a).

IV. SWITCHING BETWEEN TWO EXACTLY SOLVABLE SYSTEMS

In this section we explain the complex behavior described in Sec. III by considering the square-wave driving force with a periodic switching period $T/2$ for each of the two integrable subsystems. Each subsystem has stable and unstable fixed points for $\Gamma < 1+\mu$. For long enough T a particle al-

ways reaches the nearest fixed point and stays in it and the motion remains synchronized. But for $\Gamma > 1+\mu$, all fixed points disappear and the complex behavior shown in Fig. 2 emerges.

The two subsystems are modeled by the following dynamical equations:

$$\text{(a)}\quad \gamma\dot{x} = R(x) + \Gamma, \quad nT < t \le (2n+1)T/2,$$

$$\text{(b)}\quad \gamma\dot{x} = R(x) - \Gamma, \quad (2n+1)T/2 < t \le (n+1)T. \tag{6}$$

Note that each subsystem in Eq. (6) is modeled by a first-order ordinary nonlinear differential equation and consequently neither chaotic nor oscillatory motion is expected for each subsystem.

Both (a) and (b) in Eq. (6) may be integrated as follows:

$$t^+(x) = \int_{u=0}^{u=x} \frac{1}{v_+(u)} du,$$

$$t^-(x) = \int_{u=0}^{u=x} \frac{1}{v_-(u)} du, \tag{7}$$

with

$$v_\pm(u) = \frac{\pm\Gamma + R(u)}{\gamma}. \tag{8}$$

The integrals in Eq. (7) may be evaluated analytically for $-\pi < x < \pi$. The results are as follows:

$$t^+ = 4\mu \frac{f^+_{(1)} + f^+_{(2)}}{g^+},$$

$$f^+_{(1)} = \frac{\tanh^{-1}\frac{(1-4\mu+a)\tan(x/2)}{\sqrt{-2+8\Gamma\mu+8\mu^2-2a}}}{\sqrt{-1+4\Gamma\mu+4\mu^2-a}},$$

$$f^+_{(2)} = \frac{\tanh^{-1}\frac{(-1+4\mu+a)\tan(x/2)}{\sqrt{-2+8\Gamma\mu+8\mu^2+2a}}}{\sqrt{-1+4\Gamma\mu+4\mu^2+a}},$$

$$a = \sqrt{1-8\Gamma\mu+8\mu^2},$$

$$g^+ = \sqrt{1/2-4\Gamma\mu+4\mu^2}, \tag{9}$$

and

$$t^- = 4\mu \frac{f^-_{(1)} + f^-_{(2)}}{g^-},$$

$$f^-_{(1)} = \frac{\tanh^{-1}\frac{(1-4\mu+b)\tan(x/2)}{\sqrt{-2-8\Gamma\mu+8\mu^2-2b}}}{\sqrt{-1-4\Gamma\mu+4\mu^2-b}},$$

$$f^-_{(2)} = \frac{\tanh^{-1}\frac{-1+4\mu+b\,\tan(x/2)}{\sqrt{-2-8\Gamma\mu+8\mu^2+2b}}}{\sqrt{-1-4\Gamma\mu+4\mu^2+b}},$$

$$b = \sqrt{1+8\Gamma\mu+8\mu^2},$$

$$g^- = \sqrt{1/2+4\Gamma\mu+4\mu^2}. \tag{10}$$

The fixed points $x^*_{a,b}$ of subsystems (a) and (b) are given by

$$R(x^*)_{a,b} \pm \Gamma = 0. \tag{11}$$

The stability analysis of these fixed points is straightforward from which the following conclusions may be reached:

(1) $|\Gamma| < A[\mu + 1/(8\mu)]$ particles oscillate between two stable fixed points, one belonging to subsystem (a) and the other to subsystem (b). Consequently in this Γ range both $\langle\tilde{v}\rangle$ and $\tilde{v}_{sa}$ are equal to 0 [see Fig. 2 and see also a trajectory in Fig. 4(a)].

(2) $A[\mu+1/(8\mu)] < |\Gamma| < A[1+\mu]$. In this region subsystem (a) has no stable or unstable equilibrium points, but system (b) still has two equilibrium points in each valley (one stable and one unstable). When a periodic square-wave force (with long enough T) is applied, the particle runs to the right during the positive half cycle and goes backward to the nearest stable fixed point of system (b) during the negative half cycle. The particle stays there until the next positive half cycle. Consequently, ratchet current $\langle\tilde{v}\rangle$ is positive and increases in steps as Γ increases. Furthermore particle motion is synchronized which the driving force as the bifurcation diagram for $\tilde{v}^{sa}$ shows [see Fig. 2(b)]. $\tilde{v}^{sa}=0$ in Fig. 2(b) because in our simulations sampling is made just before the positive half cycle starts, and for those sampling times the particle rests on a fixed point of system (b) as pointed above [see also a trajectory in Fig. 4(b)].

(3) For $|\Gamma| > A[1+\mu]$ there are no longer any equilibrium points in either subsystem (a) or subsystem (b). Synchronization may be lost and the rich behavior shown in Figs. 2 and 3 becomes possible. In our simulations using $\mu=0.5$ this threshold value for $|\Gamma|$ is 1.5 [see also trajectories in Figs. 4(c) and 4(d)].

Let us now define the characteristic time τ_+ of subsystem (a) as the time required for a particle, starting at x_0, to travel a distance λ, reaching the congruent position in the next valley to the right. As explained above $|\Gamma|$ must be $> A[\mu + 1/(8\mu)]$ because for $|\Gamma| < A[\mu+1/(8\mu)]$ stable fixed points exist and the particle remains at rest instead of traveling along the ratchet.

In a similar way the characteristic time τ_- of subsystem (b) is the time required for a particle, starting at x_0, to travel a distance λ, reaching the congruent position in the next valley to the left. Now $|\Gamma|$ must be $> A[1+\mu]$ to avoid particles getting stuck in a stable fixed point.

The characteristic times may be evaluated analytically from Eqs. (9) and (10), and the results are shown in Eqs. (12) and (13),

$$\tau_+ = 2\pi \sqrt{\frac{-1+4|\Gamma|\mu+4\mu^2+4\mu\sqrt{[(|\Gamma|+\mu)^2-1]}}{[(|\Gamma|+\mu)^2-1](8|\Gamma|\mu-8\mu^2-1)}}, \tag{12}$$

$$\tau_- = 2\pi \sqrt{\frac{1+4|\Gamma|\mu-4\mu^2+4\mu\sqrt{[(-|\Gamma|+\mu)^2-1]}}{[(-|\Gamma|+\mu)^2-1](8|\Gamma|\mu+8\mu^2+1)}}. \tag{13}$$

To understand the influence of both parameters $[\Gamma, T]$ we evaluated the winding number as a function of Γ and T. The

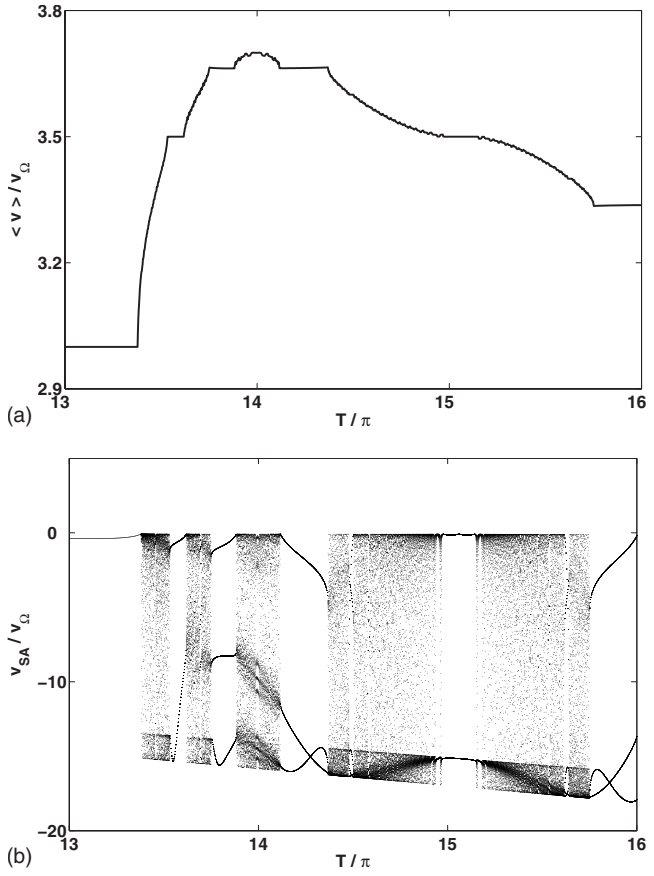

FIG. 3. (a) Mean velocity $\langle\tilde{v}\rangle$ and (b) sampled velocity $\tilde{v}_{sa}$ of a particle as a function of T for $\Gamma=1.513\simeq 1+\mu$. The particle starts at $\tilde{x}=0$.

reduced position $x_r(t)$ is the oscillation superimposed to the net transport motion. Let T_r be the period of this oscillation. Then the winding number ρ is the quotient between T and T_r [33]. As long as ρ is rational, it may be expressed as the quotient of two natural numbers: $\rho=p/q$. For this case, the motion remains synchronized with the external force. Number q amount of periods of the driving force is required to get

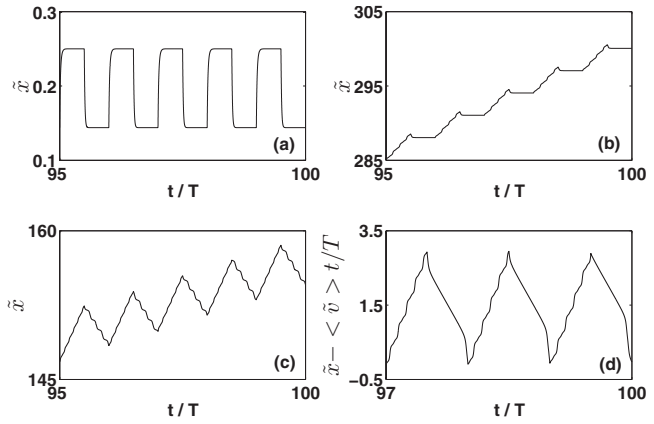

FIG. 4. (a) Trajectories for different values of parameters Γ and T: (a) $\Gamma=0.5$, $T=15.06\pi$; (b) $\Gamma=1.3$, $T=15.06\pi$; (c) $\Gamma=1.75$, $T=15.06\pi$; and (d) oscillations superimposed to the transport motion for $\Gamma=1.511$, $T=16.5\pi$.

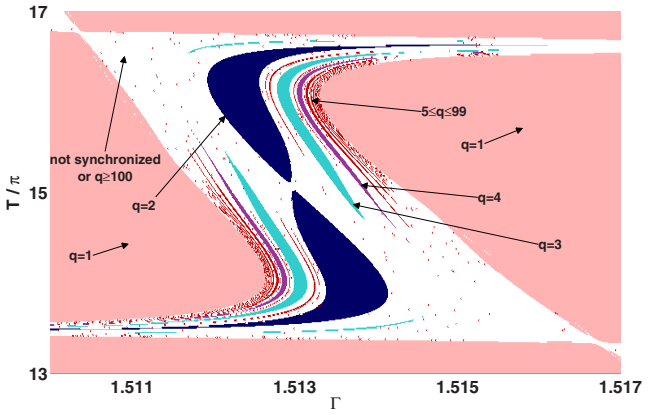

FIG. 5. (Color online) Winding number ρ as a function of Γ and T. The particle starts at $\tilde{x}=0$. Colors (or gray scale) are used for regions with a different divisor q for the winding number $\rho=p/q$: pink (light gray) corresponds to $q=1$, blue (black) corresponds to $q=2$, cyan (medium gray) corresponds to $q=3$, purple (medium gray) corresponds to $q=4$, red (dark gray) corresponds to $5<q<100$, and white (white) corresponds to $q\geq 100$. See the labels on the figure.

the same value of both the sampled reduced trajectory x_r^{sa} and the sampled velocity v^{sa}. To get the global synchronization picture shown in Figs. 5–7 we colored each zone according to the value of q. Values of q over 100 were regarded as *nonsynchronized motion* and their associated areas on the picture are colored white.

The central point of the "s-shaped" synchronization structure shown in Fig. 5 has $T\simeq 15.06\pi$ and $\Gamma\simeq 1.513$. Let us stress that the curve $\langle\tilde{v}\rangle$ vs Γ in Fig. 2(a) is a section in Fig. 5 for $T\simeq 15.06\pi$. In a similar way Figs. 3(a) and 3(b) show the bifurcation diagram for $\langle\tilde{v}\rangle$ and $\tilde{v}^{sa}$, respectively, as functions of the control parameter T for $\Gamma\simeq 1.513$ and $T\in[13\pi,16\pi]$.

To explain how synchronization is related to the characteristic times τ_+ and τ_- we have imposed a grid over the synchronization pattern for a wider region in the parameter space: $\Gamma\in[1.5,2.0]$ and $T\in[0.2\pi,20\pi]$. The dotted lines in Fig. 7 correspond to $\tau_+, 2\tau_+$, and so on as functions of Γ.

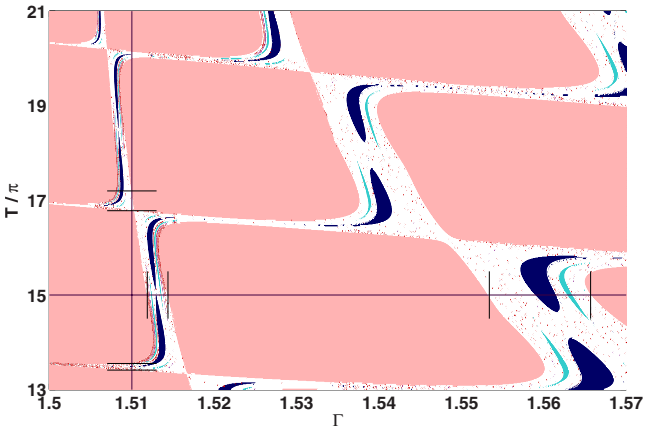

FIG. 6. (Color online) Zoom out of Fig. 5 for a wider range in parameters Γ and T. The straight lines correspond to sections used in Fig. 10

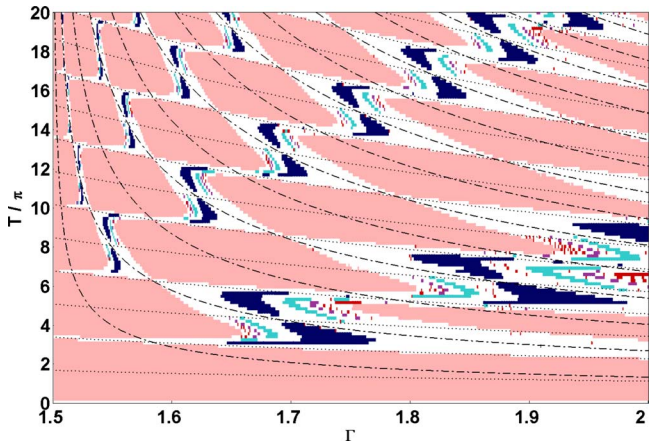

FIG. 7. (Color online) Zoom out of Fig. 5 for a wider range in parameters Γ and T. A grid corresponding to $n\tau_+$ and $n\tau_-$ as a function of Γ is superimposes over the synchronization regions.

Dashed-dotted lines correspond to $\tau_-, 2\tau_-$, and so on as functions of Γ. Each intersection between a dotted and a dashed-dotted line corresponds to a T value that is an exact multiple of both characteristic times and for these values the trajectory must be synchronized with the external driving force.

There are structurally stable as well as unstable intersection points: structurally stable intersection points have odd grid coordinates (for example, one of these points in Fig. 7 is $\tau_-, 3\tau_+$). They are surrounded by synchronization regions with $q=1$. Intersection points with both grid coordinates even (for example, $2\tau_-, 4\tau_+$) also have $q=1$ but they are structurally unstable. Finally, intersection points with one even and one odd coordinates are also unstable and they have $\rho=2$ (for example, $2\tau_-, 5\tau_+$).

V. ONE-DIMENSIONAL MAP AND BOUNDARIES OF SYNCHRONIZATION REGIONS

For each pair of values (Γ, T) the stroboscopic map $M_{\Gamma,T}=M$ may be constructed (Poincaré map) for the particle's sampled reduced position, $x_r^{sa}(n+1)=M[x_r^{sa}(n)]$. To simplify notation we will discard the superscript *sa* in this section.

The map may be determined as a composition $M=M_- \circ M_+$ of the forward map M_+ and the backward map M_-. The forward map M_+ is given by

$$M_+ : x_r(n) \to x(1/2),$$

$$\int_{u=x_r(n)}^{u=x(1/2)} \frac{1}{v_+(u)} du = T/2, \tag{14}$$

where $x(1/2)$ denotes the position, at $t=T/2$, of a particle starting at the reduced position $x_r(n)$ for subsystem (a). The backward map M_- is given by

$$M_- : x(1/2) \to x(n+1),$$

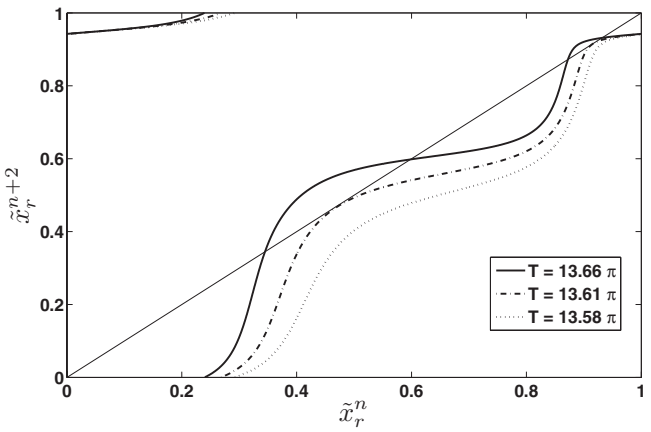

FIG. 8. A sequence of Poincaré one-dimensional iterated maps M^2 showing the tangent bifurcation for $\Gamma=1.5137$ and (a) $q=2$ orbit with $T=13.66\pi$, (b) bifurcation at $T=13.61\pi$, and (c) chaotic orbit with $T=13.58\pi$.

$$\int_{u=x(1/2)}^{u=x(n+1)} \frac{1}{v_-(u)} du = T/2, \tag{15}$$

where $x(n+1)$ is the position, at $t=T/2$, of a particle starting at the position $x(1/2)$ for subsystem (b).

The analytical expressions of the integrals above are given in Eqs. (9) and (10). Special care is required to avoid the value π in any limit of these integrals because they become singular at this point.

A stable fixed point of the j-iterated map M^j $(j=1,\ldots)$ corresponds to a synchronization region with $q=j$, as usual.

Using the one-dimensional map M, the boundary of any synchronization region may be obtained. For example, in Fig. 8, the case of a synchronization region with $q=2$ is shown. The iterated map M^2 undergoes a tangent bifurcation from $q=2$ to chaos, for $\Gamma=1.5137$, as T diminishes from $T=13.66\pi$ to $T=13.58\pi$. Another example is shown in Fig. 9 where the transition from a synchronized region with $q=1$ to chaos is considered. In this figure, the point $\Gamma=1.515$, $T=14.518\pi$ is on the boundary of the synchronization region.

Nonsynchronized regions (white regions in Fig. 5) are chaotic despite the fact that each subsystem is one dimension. We generated hundred surrogates of v^{sa} time series with 100 000 samples each for 1000 points chosen randomly inside the unstable region. For each series the distribution of the maximal Lyapunov exponents Λ was evaluated. For each series the mean value was found to be positive. For example, for $\Gamma=1.511$ and $T=16.5\pi$ the mean value of the distribution $\langle\Lambda\rangle$ is 3 and its variance σ_Λ is 0.5, confirming that the time series is chaotic.

There exists an equivalent approach for determining the boundaries of the synchronization regions. Consider, for example, a zone with $q=1$ and winding number $\rho=p/1$ (see Figs. 5 and 6). For any Γ and T inside this region, the time series of the sampled reduced position will reach, after a transitory time, a fixed point x_r^*. Correspondingly, the distance D traveled by a particle over the ratchet during the time T remains equal to $p\lambda$. This distance D is obtained as follows:

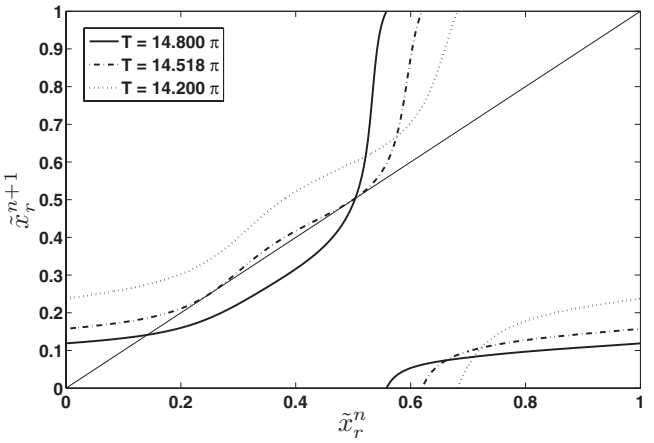

FIG. 9. A sequence of Poincaré one-dimensional iterated maps M^1 showing the transition from $q=1$ to chaos for $\Gamma=1.515$ and (a) $q=1$ orbit with $T=14.800\pi$, (b) bifurcation at $T=14.518\pi$, and (c) chaotic orbit with $T=14.200\pi$.

(1) Evaluate $x_{1/2}$ from

$$t^+ = T/2 = \int_{u=x_n}^{u=x_{1/2}} \frac{1}{v_+(u)} du. \tag{16}$$

(2) Then starting at $x_{1/2}$ evaluate x_{n+1} from $t_-=T/2$ from

$$t^- = T/2 = \int_{u=x_{1/2}}^{u=x_{n+1}} \frac{1}{v_-(u)} du. \tag{17}$$

(3) Finally, the distance D is simply $x_{n+1}-x_n$.

As x_r (the reduced position of the particle) approaches its fixed point x_r^*, the distance traveled over the ratchet approaches the value $p\lambda$ and consequently $dD\to 0$. Since D is a function of three independent variables, x, Γ and T, then inside any synchronization region the following expression holds:

$$dD = \frac{\partial D}{\partial \Gamma}\Delta\Gamma + \frac{\partial D}{\partial x}\Delta x + \frac{\partial D}{\partial T}\Delta T. \tag{18}$$

When Γ (T) change, the condition $dD=0$ may be fulfilled as far as $\frac{\partial D}{\partial x} \neq 0$ and then $\Delta\Gamma$ (ΔT) may be compensated by a finite Δx. But as parameters approach those of the boundary of the region $q=1$, $\frac{\partial D}{\partial x}$ becomes negligible and the required Δx diverges. Using Eq. (18) we can determine the boundary of region $p=1$ looking for the values of Γ (T) for which $\partial D/\partial x=0$.

In order to find and expression for $\partial D/\partial x$ let us consider a particle "a" that starts its motion at $x=x_n$. At $t=0$ the external force starts its positive half cycle. At $t=T/2$ the particle reaches position $x_{1/2}$ and the external force switches to negative. From then on the particle "a" goes back until it reaches position $x=x_{n+1}$ at $t=T$. Let us now consider another particle "b" starting its motion at $x=x_n+\Delta x$. At $t=T/2$ this particle "b" will reach position given by

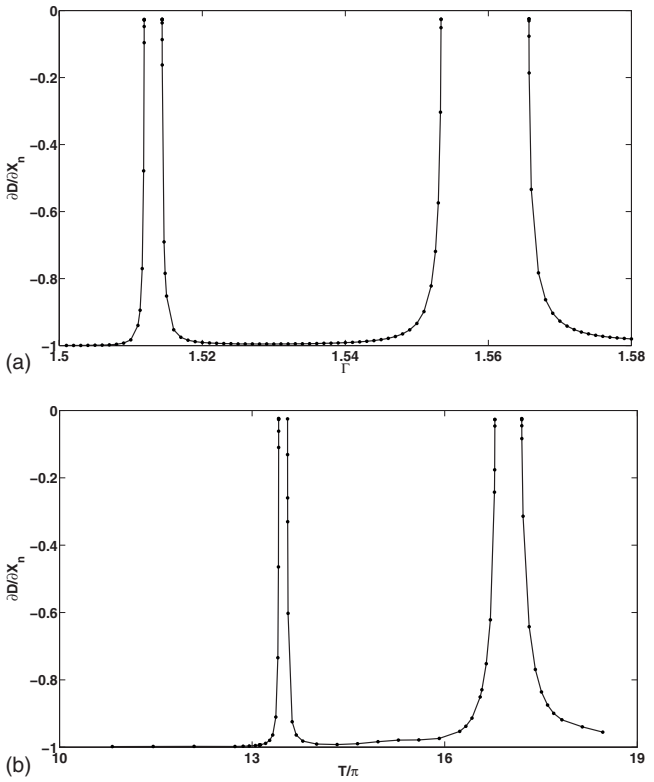

FIG. 10. (a) $\partial D/\partial x_n$ as a function of Γ for $T=15\pi$ (see horizontal straight lines in Fig. 6). (b) $\partial D/\partial x_n$ as a function of T for $\Gamma=1.51$ (see vertical straight lines in Fig. 6).

$$x_{1/2}^b = x_{1/2} + \frac{v_+(x_{1/2})}{v_+(x_n)}\Delta x. \tag{19}$$

By going on with this method it can be easily demonstrated that

$$\Delta D = (x_{n+1}^b - x_n^b) - (x_{n+1} - x_n) \tag{20}$$

$$= \left[\frac{v_-(x_{n+1})v_+(x_{1/2})}{v_+(x_n)v_-(x_{1/2})} - 1\right]\Delta x \tag{21}$$

and

TABLE I. Transitory time as a function of α for $\Gamma=1.730\,63$ and $T\simeq 14.90\pi$ on the border of a chaotic region (see Fig. 5).

α	q	T_{trans}/T
0.990	1	62
0.991	1	68
0.992	1	75
0.993	1	85
0.994	1	98
0.995	1	118
0.996	1	154
0.997	1	277
0.998	1	>1000
0.999	1	>1000

$$\frac{\partial D}{\partial x} = \frac{v_-(x_{n+1})v_+(x_{1/2})}{v_+(x_n)v_-(x_{1/2})} - 1. \tag{22}$$

For $x=x^*$,

$$\frac{\partial D}{\partial x^*} = \frac{v_-(x^*)v_+(x_{1/2})}{v_+(x^*)v_-(x_{1/2})} - 1. \tag{23}$$

Then the boundary corresponds to the following condition:

$$\frac{v_-(x^*)v_+(x_{1/2})}{v_+(x^*)v_-(x_{1/2})} - 1 = 0, \tag{24}$$

which leads to

$$R(x^*) = R(x_{1/2}). \tag{25}$$

Figure 10(a) shows $\partial D/\partial x$ for constant $T=15\pi$ and variable Γ (see the horizontal straight line in Fig. 6). The boundary corresponds to the value of Γ that makes $\partial D/\partial x=0$. In a similar way Fig. 10(b) shows $\partial D/\partial x$ for constant $\Gamma=1.51$ and variable T (see the vertical straight line in Fig. 6). The boundary corresponds to the value of T that makes $\partial D/\partial x=0$.

Using this analysis it is easy to prove that the intersection points of the grid in Fig. 7 corresponding to odd multiples of both τ_+ and τ_- are structurally stable. To see this, consider the intersection between $(i\tau_+)$ and $(j\tau_-)$ with both i and j odd integers. For a particle starting at $x_n=0$, $x_{1/2}=i\lambda/2$ and $x_{n+1}=(i-j)\lambda/2$. Then, x_{n+1} is congruent to x_n and also to $x=0$. Furthermore, $R(x_n)=1.5\neq R(x_{1/2})=-0.5$. Therefore, the point does not belong to the boundary and the system is structurally stable.

A discontinuous force is a singular function. Real square waves are smooth and if a smooth function is used as driving force the existence and uniqueness theorem precludes chaos in our model. Then the robustness of our results must be analyzed. A smooth square force may be constructed as follows:

$$F(t) = \begin{cases} +\Gamma \sin[2\pi t_r/\{(1-\alpha)\}T] & \text{if } t_r < (1-\alpha)T/4 \\ +\Gamma & \text{if } (1-\alpha)T/4 \le t_r \le T/2-(1-\alpha)T/4 \\ -\Gamma \sin[2\pi(t_r-T/2)/\{(1-\alpha)T\}] & \text{if } T/2-(1-\alpha)T/4 < t_r < T/2+(1-\alpha)T/4 \\ -\Gamma & \text{if } T/2+(1-\alpha)T/4 \le t_r \le T-(1-\alpha)T/4 \\ +\Gamma \sin[2\pi(t_r-T)/\{(1-\alpha)T\}] & \text{if } t_r > T-(1-\alpha)T/4, \end{cases} \tag{26}$$

where $0\le\alpha\le 1$ is the control parameter of the connection steepness and $t_r=(t \bmod T)$. When this $F(t)$ is used instead of that in Eq. (3) the system will reach a synchronized state but for parameter values $[\Gamma, T]$ corresponding to chaotic regions (white regions of Figs. 5–7) the transitory times tend to infinity as α approaches 1 (discontinuous case). Table I shows this effect. Consequently our results will be observed, in practical, in experimental cases using realizable rectangular forces.

VI. CONCLUSIONS

In summary, a rich complex behavior including synchronization and chaos is presented in this paper for an overdamped ratchet forced by a square wave. Finite inertia terms or temporal or spatial stochastic forces, commonly associated with a chaotic behavior, are not present in our model. The bifurcation diagram of the winding number reveals an interesting structure, induced by the switching process, with synchronization regions of different periods as well as chaotic regions. A grid using the characteristic times τ_+ and τ_- as coordinates was used to characterize it systematically. Results are robust in the sense that transitory times increase without limit as *smooth* square force approaches the discontinuous case. The results presented in this paper, particularly the existence of bifurcations and chaos, may be experimentally confirmed in a number of experiments, including the three-junction SQUID ratchet [8], the rocking ratchet effect for cold atoms [14], and the Josephson vortex ratchet [12].

ACKNOWLEDGMENTS

This work was partially supported by CONICET (Grant No. PIP 5569), Universidad Nacional de Mar del Plata, and ANPCyT (Grant Nos. PICT 11-21409, PICT 008907, and PICTO 11-495).

[1] R. D. Astumian and M. Bier, Phys. Rev. Lett. **72**, 1766 (1994).
[2] F. Jülicher, A. Ajdari, and J. Prost, Rev. Mod. Phys. **69**, 1269 (1997).
[3] J. M. R. Parrondo, L. Dinís, J. Buceta, and Katja Lindenberg, in *Advances in Condensed Matter and Statistical Physics*, edited by E. Korutcheva and R. Cuerno (Nova Science, New York, 2003).
[4] R. Gommers, S. Denisov, and F. Renzoni, Phys. Rev. Lett. **96**,

240604 (2006).
[5] A. B. Kolton, Phys. Rev. B **75**, 020201(R) (2007).
[6] A. Pérez-Junquera, V. I. Marconi, A. B. Kolton, L. M. Álvarez-Prado, Y. Souche, A. Alija, M. Vélez, J. V. Anguita, J. M. Alameda, J. I. Martín, and J. M. R. Parrondo, Phys. Rev. Lett. **100**, 037203 (2008).
[7] I. Zapata, R. Bartussek, F. Sols, and P. Hänggi, Phys. Rev. Lett. **77**, 2292 (1996).
[8] A. Sterck, R. Kleiner, and D. Koelle, Phys. Rev. Lett. **95**, 177006 (2005).
[9] G. Carapella and G. Costabile, Phys. Rev. Lett. **87**, 077002 (2001).
[10] J. F. Wambaugh, C. Reichhardt, C. J. Olson, F. Marchesoni, and F. Nori, Phys. Rev. Lett. **83**, 5106 (1999).
[11] C. J. Olson, C. Reichhardt, B. Jankó, and F. Nori, Phys. Rev. Lett. **87**, 177002 (2001).
[12] M. Beck, E. Goldobin, M. Neuhaus, M. Siegel, R. Kleiner, and D. Koelle, Phys. Rev. Lett. **95**, 090603 (2005).
[13] M. Kostur, L. Machura, P. Talkner, P. Hänggi, and J. Luczka, Phys. Rev. B **77**, 104509 (2008).
[14] M. Brown and F. Renzoni, Phys. Rev. A **77**, 033405 (2008).
[15] P. H. Jones, M. Goonasekera, D. R. Meacher, T. Jonckheere, and T. S. Monteiro, Phys. Rev. Lett. **98**, 073002 (2007).
[16] S. J. Lade, J. Phys. A: Math. Theor. **41**, 275103 (2008).
[17] J. R. Chaudhuri, D. Barik, and S. K. Banik, J. Phys. A: Math. Theor. **40**, 14715 (2009).
[18] L. Machura, J. Luczka, P. Talkner, and P. Hänggi, Acta Phys. Pol. B **38**, 1855 (2007).
[19] Bao-Quan Ai and Liang-Gang Liu, J. Chem. Phys. **126**, 204706 (2007).
[20] F. R. Alatriste and J. L. Mateos, Physica A **372**, 263 (2006).
[21] J. L. Mateos and F. R. Alatriste, Chaos **18**, 043125 (2008).
[22] A. Pikovsky, M. Rosenblum, and J. Kurths, *Synchronization: A Universal Concept in Nonlinear Sciences*, Cambridge Nonlinear Science Series Vol. 12 (Cambdridge University Press, Cambdridge, 2001).
[23] S. H. Strogatz, *Nonlinear Dynamics and Chaos: With Applications to Physics, Biology, Chemistry, and Engineering* (Addison-Wesley, Cambridge, MA, 1994).
[24] M. N. Popescu, C. M. Arizmendi, A. L. Salas-Brito, and F. Family, Phys. Rev. Lett. **85**, 3321 (2000).
[25] M. F. Shlesinger, G. M. Zaslavsky, and J. Klafter, Nature (London) **363**, 31 (1993).
[26] L. Gao, X. Luo, S. Zhu, and B. Hu, Phys. Rev. E **67**, 062104 (2003).
[27] D. G. Zarlenga, H. A. Larrondo, C. M. Arizmendi, and F. Family, Physica A **352**, 282 (2005).
[28] D. G. Zarlenga, H. A. Larrondo, C. M. Arizmendi, and F. Family, Phys. Rev. E **75**, 051101 (2007).
[29] P. Jung, J. G. Kissner, and P. Hänggi, Phys. Rev. Lett. **76**, 3436 (1996).
[30] J. L. Mateos, Phys. Rev. Lett. **84**, 258 (2000).
[31] M. Barbi and M. Salerno, Phys. Rev. E **62**, 1988 (2000).
[32] C. M. Arizmendi, F. Family, and A. L. Salas-Brito, Phys. Rev. E **63**, 061104 (2001).
[33] H. A. Larrondo, F. Family, and C. M. Arizmendi, Physica A **303**, 67 (2002).
[34] H. A. Larrondo, C. M. Arizmendi, and F. Family, Physica A **320**, 119 (2003).
[35] F. Family, H. A. Larrondo, D. G. Zarlenga, and C. M. Arizmendi, J. Phys.: Condens. Matter **17**, S3719 (2005).
[36] U. E. Vincent, A. Kenfack, A. N. Njah, and O. Akinlade, Phys. Rev. E **72**, 056213 (2005).
[37] U. E. Vincent, A. N. Njah, and J. A. Laoye, Physica D **231**, 130 (2007).
[38] W. S. Son, J. W. Ryu, D. U. Hwang, S. Y. Lee, Y. J. Park, and C. M. Kim, Phys. Rev. E **77**, 066213 (2008).
[39] R. Salgado-García, M. Aldana, and G. Martínez-Mekler, Phys. Rev. Lett. **96**, 134101 (2006).
[40] R. Salgado-García, G. Martínez-Mekler, and M. Aldana, Phys. Rev. E **78**, 011126 (2008).
[41] X. Liu, K.-L. Teo, H. Zhang, and G. Chen, Chaos, Solitons Fractals **30**, 725 (2006).
[42] S. I. Denisov, M. Kostur, E. S. Denisova, and P. Hänggi, Phys. Rev. E **76**, 031101 (2007).
[43] Xiaoqun Wu, Xiaoqun Wang, Jun-an Lu, and Herbert H. C. Iu, Chaos, Solitons Fractals **32**, 1485 (2007).
[44] E. Gluskin, e-print arXiv:0801.3652 (2008).
[45] D. Cubero, J. Casado-Pascual, A. Alvarez, M. Morillo, and P. Hänggi, Acta Phys. Pol. B **37**, 1467 (2006).
[46] W. H. Press, S. A. Teikolsky, W. T. Vetterling, and B. P. Flannery, *Numerical Recipes in C* (Cambridge University Press, Cambridge, 1995).